Initial Precipitation Formation in Warm Florida Cumulus

NEIL F. LAIRD AND HARRY T. OCHS III

Atmospheric Environment Section, Illinois State Water Survey, Champaign, Illinois

ROBERT M. RAUBER

Department of Atmospheric Sciences, University of Illinois, Urbana–Champaign, Urbana, Illinois

L. JAY MILLER

Mesoscale and Microscale Meteorology Division, National Center for Atmospheric Research, Boulder, Colorado

(Manuscript received 21 April 1999, in final form 13 March 2000)

ABSTRACT

The microphysical processes that lead to the development of precipitation in small, warm cumulus are examined using data from the Small Cumulus Microphysics Study near Cape Canaveral, Florida. Aircraft measurements are used to determine the concentration and size distribution of giant and ultragiant nuclei in clear air as a function of relative humidity, altitude, wind speed, and wind direction. The clear-air particle distributions show that ultragiant particles (radii extending from 10 to 150 μm) exist from the surface to cloud base in concentrations that correspond to the concentrations of raindrops observed during drizzle to moderate rainfall events. A shift of the spectra toward larger size with increasing relative humidity was observed, suggesting that the spectra are composed of deliquesced particles growing by condensation. The small cumulus clouds are shown to contain cores where the observed liquid water content was nearly adiabatic. The observed evolution of the cloud droplet distribution within the near-adiabatic cores as a function of height showed an increase in the small droplet mode associated with condensation and an increase in the concentration of larger droplets associated with growth by accretion. Droplets with radii extending to nearly 100 μm were present just above cloud base. These measurements were consistent with the clear-air measurements and provided evidence that the ultragiant nuclei can immediately act as embryos for raindrop growth by accretion upon entering cloud base. Comparisons of reflectivity computed from the cumulus core composite droplet distributions with the radar-observed reflectivity data provided independent evidence that the composite spectra reasonably represented the evolving microstructure of the cores of small cumulus clouds as they grew vertically.

The analyses provide strong evidence of an efficient process for the initial development of precipitation in small Florida cumuli. This process consists of raindrop embryo formation on ultragiant nuclei followed by growth by accretion as the newly formed drops proceed upward through the adiabatic cores of the cumulus clouds. These data support the conceptual model of raindrop formation in marine clouds first proposed by Woodcock a half century ago.

1. Introduction

One of the major unresolved scientific issues in cloud physics is the explanation of the observed short time between initial cloud formation and the onset of precipitation in warm (>0°C) clouds. Whatever the growth processes, they must be fast enough to account for growth from condensation nuclei to raindrops in about 15–20 min. Although diffusional growth theory can adequately explain the early stages of cloud drop development with narrow size distributions, it cannot account for the broadening with time of the drop size distribution that has been observed in clouds. Several hypotheses have been developed to explain the broadening of droplet size distributions, a requirement for the onset of collision–coalescence. Hypotheses include mechanisms that enhance condensation growth of a few larger cloud droplets through 1) mixing (Ludlam and Saunders 1956; Latham and Reed 1977; Baker and Latham 1979; Telford et al. 1984; Cooper et al. 1986; Politovich and Cooper 1988), 2) fluctuations in supersaturation or collision rates induced by turbulence (Khain and Pinsky 1995), and 3) recirculation of growing drops (Rauber et al. 1991; Kogan 1993). Other mechanisms for drop spectral broadening have been proposed—namely, ir-

Corresponding author address: Neil F. Laird, Illinois State Water Survey, 2204 Griffith Drive, Champaign, IL 61820-7495.
E-mail: n-laird@uiuc.edu

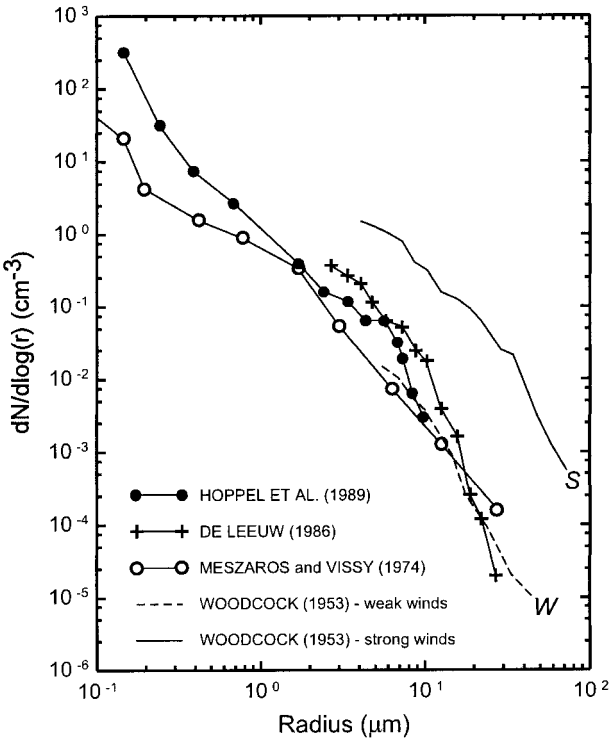

FIG. 1. Comparison of clear-air particle distributions in marine environments. Meszaros and Vissy (1974), filter samples at 76% RH; de Leeuw (1986), inertial impactor at 68% RH; Hoppel et al. (1989), replicator impactor at 75% RH; and for the weak (W) and strong (S) wind force cases of Woodcock (1953), glass slides at 99% RH.

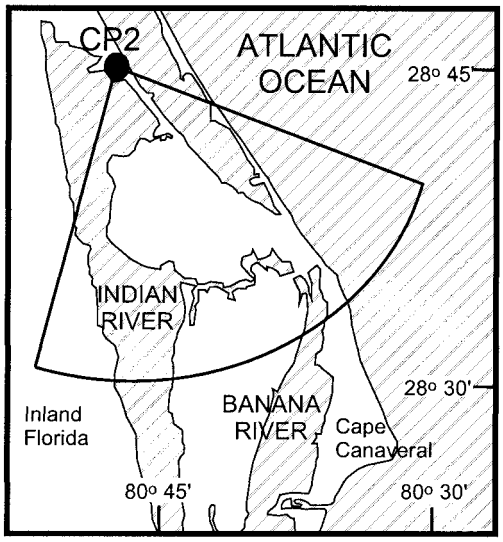

FIG. 2. SCMS primary study region. Sector shows region where radar and aircraft coordinated measurements within small cumulus.

reversibility in droplet growth resulting from solute and curvature effects (Korolev 1995), and radiational cooling (e.g., Austin et al. 1995).

One of the simplest hypotheses to explain the onset of precipitation in warm clouds is that ultragiant particles (>10-μm dry radius), such as wettable or soluble sea-salt nuclei, are the embryos for the first raindrops (e.g., Woodcock and Gifford 1949; Ochs and Semonin 1979; Johnson 1982, 1993). These particles, when carried through cloud base, can almost immediately begin to grow by collecting cloud droplets (Johnson 1979). Even though this process can lead to the development of large raindrops in the observed times of 15–20 min (Szumowski et al. 1999), questions remain as to whether the concentration of these large salt particles is sufficient to account for the onset of rain in maritime clouds (e.g., Mordy 1959; Woodcock et al. 1971; Rogers and Yau 1989).

In marine environments, sulfate aerosols are known to be the primary source of cloud condensation nuclei (e.g., Charlson et al. 1987; Hegg et al. 1991; Hoppel 1987) and control the initial condensation process. However, it has been observed that larger particles ($r > 0.5$ μm) are almost entirely composed of sea-salt aerosols. Woodcock (1953), for example, measured sea-salt aerosol concentrations near cloud base in the range of 10^{-3}–10^{-5} cm^{-3} for salt particles with $r > 10$ μm at 99% relative humidity during modest surface winds of 3.5–8.0 m s^{-1}. Reviews by Fitzgerald (1991) and O'Dowd et al. (1997) of several studies of marine aerosol distributions support some of the earlier observations of Woodcock (1953). Figure 1 shows a comparison of the particle size distributions of marine aerosol from studies that used a variety of instrumentation in different oceanic regions. These results show that concentrations of marine aerosol with radii greater than 10 μm range from 10^{-2} to 10^{-5} cm^{-3}. If ultragiant aerosols are present in these concentrations, they should contribute to the large end of the droplet spectrum and lead to efficient collision–coalescence drop growth.

In addition to the existence of ultragiant particles, the cloud environment must also support rapid particle growth to explain the formation of rain in 15–20 min. The cloud liquid water content (LWC) is fundamental in controlling the rate at which the warm-rain process proceeds. Recent modeling results by Feingold et al. (1999) for stratocumulus clouds show that the maximum relative effect of giant cloud condensation nuclei (CCN) on the collision–coalescence process occurs for total CCN concentration (N) and LWC that vary in tandem, that is, large N and large LWC, or small N and small LWC. It has proven to be difficult to adequately and reliably measure LWC (Beard and Ochs 1993). Early studies of marine clouds generally showed the LWC to be about half adiabatic (e.g., Warner 1955). However, a study by Lawson and Blyth (1998) recently demonstrated that several of the small Florida cumulus clouds observed during the Small Cumulus Microphysics Study (SCMS) contained regions where the observed LWC was very close to adiabatic.

The SCMS, conducted in 1995 along the east central coast of Florida in the vicinity of Cape Canaveral (Fig. 2), used three research aircraft [a C130 from the Na-

tional Center for Atmospheric Research (NCAR), a King Air from the University of Wyoming, and a Merlin from Meteo-France] along with the dual-wavelength NCAR CP2 radar to obtain measurements necessary to explain the onset of precipitation in warm cumulus. A large suite of probes was carried on the C130 in order to accurately measure the complete distribution of drop sizes from very small cloud drops (≥ 3 μm) to raindrops (about 1 mm). These probes also provided measurements of particle sizes within the optically clear air. The radar was used to obtain complete cloud histories.

In this article, we use SCMS aircraft measurements to determine 1) the concentration and size distribution of ultragiant nuclei in clear air as a function of relative humidity, altitude, wind speed, and wind direction (section 3); 2) whether adiabatic and near-adiabatic cumulus cores exist; and 3) the cloud drop size distribution and vertical motions within the cores as a function of altitude (section 4). From the observed X-band radar reflectivity factor (hereafter called reflectivity), we establish the time from earliest radar echo (about -20 dBZ) until rainout (about one 1-mm drop per cubic meter or 0 dBZ). We also use the radar-observed reflectivities to provide a quantitative comparison with reflectivities calculated from aircraft measurements in near-adiabatic cumulus cores (section 5).

In a later article, the data and results presented here will be used for initialization and validation of numerical simulations of drop growth in clouds with and without ultragiant nuclei using a modified version of the Ochs and Yao (1978) moment-conserving parcel model. This combined observational, numerical modeling approach provides a test of the hypotheses that ultragiant particles, presumably sea-salt nuclei, are responsible for the rapid onset of precipitation in the warm Florida cumulus clouds observed during SCMS.

2. Measurements and methods

Measurements from the NCAR C130 aircraft and the NCAR CP2 dual-wavelength radar (3 and 10 cm) were the primary sources of data for this study. The aircraft measurements were averaged to 1 Hz corresponding to a distance of approximately 105 m. The instrumentation used to examine the cloud LWC and particle size distributions in this article include a Particle Measuring Systems (PMS) forward scattering spectrometer probe (FSSP-100) and a PMS 260X optical array probe (Knollenberg 1981). The size range of the FSSP was varied during the project, but was typically set at the broadest range (nominally 3–48-μm diameter in 15 size bins) with a sample volume of 0.53 cm^3 for 1 m of flight distance. The data presented in this article are from time periods when this size range was used. The FSSP measurements from other time periods were found to be consistent with the data presented here. Baumgardner (1989) and Lawson and Blyth (1998) describe the corrections and calibrations applied to the FSSP data. The 260X optical array probe for SCMS was adjusted to measure drop sizes in 60 usable bins of 17-μm width ranging from 51- to 1054-μm diameter and had a maximum sample volume of 47.9 cm^3 for 1 m of flight distance. In addition, the 260X probe was fitted with antishedding tips to prevent artifacts from contaminating the measurements.

Because of the low concentrations for the clear-air particles, we accumulated bin concentrations over many 1-Hz samples to increase the size of the sample volume associated with the original 1-Hz data. The clear-air aerosol distributions that we present in this article are composites of data from outside of cloud during 12 project flights. The particles were sampled in situ at ambient relative humidity. Particle sizes reported are the sizes at the ambient relative humidity. No adjustments were made to account for the possibility that the particles may not have been at their equilibrium size. Determining time periods when the C130 was outside of cloud was completed to the degree possible using measurements independent of the FSSP and 260X, since these instruments were used to determine the particle size distributions. Forward-looking flight video recordings from each flight were used to make an initial determination of time periods when the aircraft was located in clear-air regions. These segments of the flights typically were over either the Atlantic Ocean, the Indian and Banana Rivers, the shoreline side of the sea-breeze front, or at least 150 m below cloud base (Fig. 2). We were conservative in choosing time periods when the aircraft was outside of cloud. Time periods when the aircraft was closer than about 1.5 km to a cloud edge were rejected. If it was evident that the C130 was near or within a cloud field, the data was not included in our clear-air analyses. This procedure ensured that none of the detected particles could have been drops ejected from the tops of nearby clouds or that measurements were collected within the area where a cloud recently evaporated. The clear-air time periods selected from the videos were additionally examined for possible cloud contamination using all available aircraft measurements of cloud properties, such as FSSP derived LWC, PMS King probe LWC, Gerber Scientific probe LWC, and total particle concentrations from the 260X and FSSP. From the 12 flights, the follow-up examination of in situ measurements led to the identification of only two short time periods that contained questionable data. These periods were eliminated from the analyses.

Since a significant part of our interpretation of the SCMS data depends on the measurements of the C130 FSSP and 260X particle probes in clear air, it is incumbent upon us to first test the hypothesis that the clear-air signal from the FSSP and 260X probes were created by instrumentation noise rather than particles. Our test involves a search for two indicators of noise. If the signal were white noise with a large sample, one would expect a uniform distribution of counts across all size channels of each instrument. The second indicator

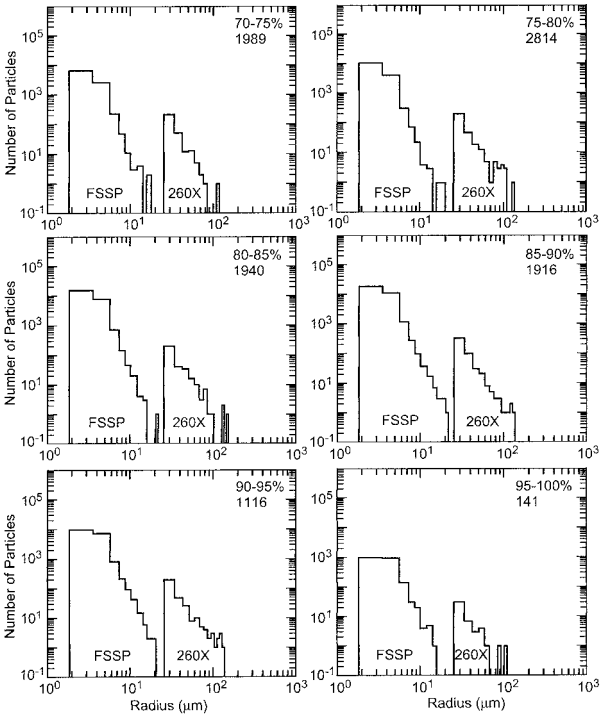

FIG. 3. SCMS clear-air composite particle count distributions derived using FSSP and 260X measurements as a function of relative humidity. The numbers of 1-Hz samples that are included in each composite are shown.

would be that the noise was confined to a specific size channel(s) of each instrument. This noise would result in anomolously high counts in the specific channel(s) affected by the noise. Figure 3 shows the distribution of clear-air raw counts from both the C130 FSSP and 260X probes composited over the 12 flights included in the analysis. Similar distributions were obtained for individual flights during SCMS. The distribution of counts shows an exponential behavior in both probes, implying that the signal is unlikely to be associated with white noise. In addition, particle counts are not distributed across all size channels of the 260X probe but are only present in size channels less than about 200 μm-radius. There are no spikes in the distribution, a signal that would be characteristic of a probe malfunction that would lead to repeated triggering of a signal in a specific size bin. Since the indicators of noise do not exist in the C130 data, we conclude that the FSSP and 260X probes are responding to particles in the atmosphere. Of course, instrument bias and errors may still remain, but there is little doubt that the ultragiant particle spectra extends to sizes greater than 100-μm radius.

Knight and Miller (1993, 1998) describe the use of the NCAR CP2 dual-wavelength radar to examine early radar echoes from small, warm cumulus. During SCMS the CP2 radar had a pulse length of 150 m and operated primarily in the range–height indicator (RHI) scan mode with scans spaced every 1°–1.5° in azimuth. Using this scanning strategy, a complete scan of the cloud volume took approximately 2 min. Knight and Miller (1998) provide a detailed description of the radar parameters and scanning strategy of the CP2 radar during SCMS, as well as corrections applied to the data. The two radars (3 and 10 cm) are sensitive to both Bragg and Rayleigh scattering. The 3-cm wavelength reflectivity is predominantly due to Rayleigh scattering and is therefore more directly related to the drop size distribution. For the purposes of this article, it was unnecessary to correct the 3-cm reflectivity for the small amount of Bragg scattering.

The clouds sampled during SCMS had short lifetimes (20–25 min). Logistics associated with radar and aircraft sampling limited the number of observations of any cloud. Typically the C130 made one to three passes at one altitude through a given cloud. These passes may or may not have been through the cumulus core. Approximately five radar volumes were typically collected for a cloud during its lifetime. The aircraft rarely sampled a cloud at the same time and location that the radar scanned the cloud, and when this did occur the radar signal was overwhelmed by the return signal from the aircraft. For these reasons it was difficult to obtain meaningful in situ results from studies of the evolution of individual clouds.

Our approach was to composite all penetrations of clouds that contained near-adiabatic cores during SCMS. This greatly improved the sampling statistics (Cornford 1967) for the drop size distributions, particularly for the larger droplets, which have low concentrations. By limiting the data used to derive the composite drop distributions to penetrations of near-adiabatic cores, we are primarily including penetrations through clouds during their development stage. Although the ambient environment showed some interday variability, a drawback to the compositing approach, the interday variations in the environment along the east coast of Florida on the days included in this study were generally not substantial.

In order to examine the measurements of cloud LWC from the FSSP in a meaningful way, the entire SCMS C130 FSSP dataset was compared to calculated adiabatic values of LWC. The LWC of a parcel that ascends adiabatically from cloud base was calculated for each day using information measured within the surface mixed layer during the initial ascent of the C130. The surface mixed layer was defined as the layer nearest the surface where the mixing ratio and equivalent potential temperature remain nearly constant with height. At the time of takeoff, the top of the surface mixed layer was generally below 0.2 km. The cloud base temperature and pressure were estimated using the pressure, temperature, and dewpoint temperature near the 50-m level; an empirical formulation for the temperature of cloud base (Inman 1969); the dry adiabatic lapse rate; and the hydrostatic equation. The adiabatic LWC profile was then calculated by iteratively integrating the equation

for psuedomoist adiabatic lift (Eq. 1), using an empirical equation for saturation vapor pressure over water (Pruppacher and Klett 1978), and then subtracting the saturation mixing ratio at each new level from that at cloud base:

$$0 = C_p\, d\ln T - R_d\, d\ln P + d(L_v r_s/T). \qquad (1)$$

In Eq. (1), C_p is the specific heat of dry air at constant pressure, R_d is gas constant for dry air, L_v is latent heat of vaporization, T is air temperature, P is pressure, and r_s is the saturation mixing ratio.

Cloud-base height at a specific time is often a difficult quantity to accurately determine. For example, Knight and Miller (1998) show a 0.2-km uncertainty in the position of cloud base (0.7–0.9 km) estimated from the CP2 radar. Visual observations of cloud-base height from forward-looking flight video recordings suggest that cloud-base height often varied slightly over the duration of a research flight and with changes in land surface properties, such as river, ocean, land, and wetlands that make up the Cape Canaveral shoreline region. In general, in situ measurements of cloud-base temperature and pressure available from C130 flights compared well with estimates determined from mixed layer parameters. Estimated cloud-base height was generally found to be equal to or slightly higher than measured cloud-base height. The uncertainty in cloud-base temperature and pressure were approximately 0.5°–1.0°C and 10–15 hPa. Lawson and Blyth (1998) found that for typical cloud-base conditions during SCMS of 950 hPa and 23°C, an uncertainty of +10 hPa and +1°C can result in an overestimate of adiabatic LWC by about 0.2 and 0.1 g m^{-3}, respectively. A comparison of estimated cloud-base height from mixed layer parameters collected during C130 initial ascents and landings indicates that cloud-base height, in some cases, remained nearly constant [approximately 0.7 km (i.e., 960 hPa)], while in other cases it increased by as much as 0.3 km during flight. An increase of cloud-base height with time suggests that our calculations of adiabatic LWC (calculated from initial ascent mixed layer parameters) may be overestimated and therefore provide a conservative LWC for comparison with measured LWC from cumulus penetrations during the later portion of some flights.

3. Clear-air particle size distributions and total concentrations

a. SCMS relative humidity composite

Figure 4 shows composite particle size distributions derived using FSSP and 260X measurements in clear-air regions as a function of relative humidity (RH). Spectra are shown for relative humidities from 70% to 100% in 5% intervals. The distribution for 70%–75% RH is overlaid on the distribution for 90%–95% RH for ease of comparison. The numbers of 1-Hz samples averaged to form each distribution are also shown. The sea-salt nuclei size data reported by Woodcock (1953) at 99% RH for weak (W: 0.3–1.5 m s^{-1}) and strong (S: 13.9–17.1 m s^{-1}) winds in the vicinity of Hawaii are overlaid for reference. The SCMS data included in these composite distributions were collected between the surface and 0.8 km during 12 flights and include data for *all* wind speeds and directions. Figures 3 and 4 show that as the RH increases, the FSSP measures a consistent increase in the average particle counts (i.e., total counts divided by number of samples) and composite particle concentrations, respectively. The SCMS FSSP particle concentrations increase toward the weak-wind sea-salt particle distribution of Woodcock (1953). The 260X particle concentrations also increase at higher RH. Figure 4 demonstrates that particles with radii $>100\mu$m are present at relative humidities >70% in the Florida environment.

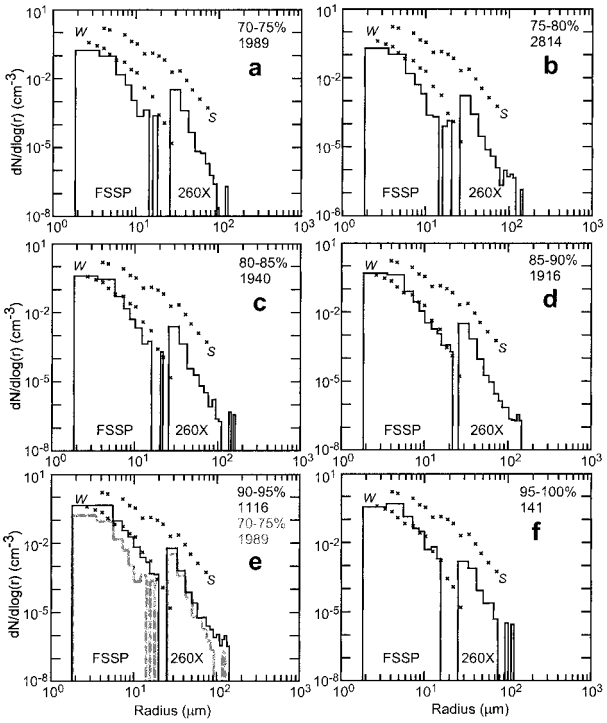

FIG. 4. SCMS clear-air composite particle size distributions as a function of relative humidity derived using FSSP and 260X measurements. The number of 1-Hz samples that are included in each composite are shown. In each panel, the sea-salt nuclei size data collected by Woodcock (1953) for weak (W: 0.3–1.5 m s^{-1}) and strong (S: 13.9–17.1 m s^{-1}) wind cases in the vicinity of Hawaii are overlaid for reference.

The compositing method greatly improved the sampling statistics for the clear-air particle size distributions, particularly for the larger particles, which have low concentrations. Cornford (1967) showed that the true concentration for a finite particle size range lie within 50% of the sampled concentration with a 95% confidence provided that there are at least seven particles measured. Using Cornford's (1967) statistical approach and the

accumulated particle count from Fig. 3, the uncertainty in the concentration of particles in the size range near 100-μm radius on the distributions shown in Fig. 4 is approximately a factor of 2 with 95% confidence. At smaller sizes the uncertainty is much less since many more particles were sampled. The major source of uncertainty in these measurements is not the sampling statistics but rather instrument error and bias. As is evident from Fig. 4, comparison of the slopes of the distributions from the 260X and FSSP show a potential 2 order of magnitude difference in the measured concentrations of particles. This offset may be due to optical properties of the clear-air particles measured, although the sources of the difference are unknown. However, comparisons of independent measurements of particle size distributions in marine environments (Fig. 1) with the distributions from the 260X and FSSP show that SCMS measurements straddle the distributions obtained by other researchers. It is difficult to determine the extent to which the differences in the size distributions are due to differences in geographic location and meteorological conditions such as wind speed or to errors inherent in different measurement techniques.

To determine the level of significance of the difference between concentrations at different relative humidities, standard statistical tests were performed to compare particle concentrations within individual size bins. A statistical *t* test was performed that uses the standard deviation of the 1-Hz concentrations in each size bin of the composite spectra to estimate the level of significance of the difference between concentrations in corresponding size bins. The compositing approach provided sufficiently large sample sizes and allowed for the use of this statistical method. Composite clear-air SCMS particle distributions shown in Figs. 4a–d were compared to the 90%–95% RH particle distribution (Fig. 4e). The results show that the concentrations of particles $\leq$6-μm radius at 70%–75% and 75%–80% RH are significantly different from those at 90%–95% RH at a 95% confidence level. Particle concentrations within other size intervals and at other relative humidities were not significantly different at a 95% confidence level when compared to the particle size distribution at 90%–95% RH. Although the differences in concentrations in the individual size bins were not statistically significant, the consistency in the overall shift of the spectra toward larger size as a function of increasing RH lends confidence to the conclusion that the spectra are composed of deliquesced particles growing by condensation.

b. SCMS height composite

Figure 5 shows the composite particle size distributions derived using FSSP and 260X measurements in clear-air regions within 0.2-km layers from the surface to 0.8 km. The numbers of 1-Hz samples averaged in each distribution are also shown. The SCMS data included in these composite distributions are the same as those used in section 3a.

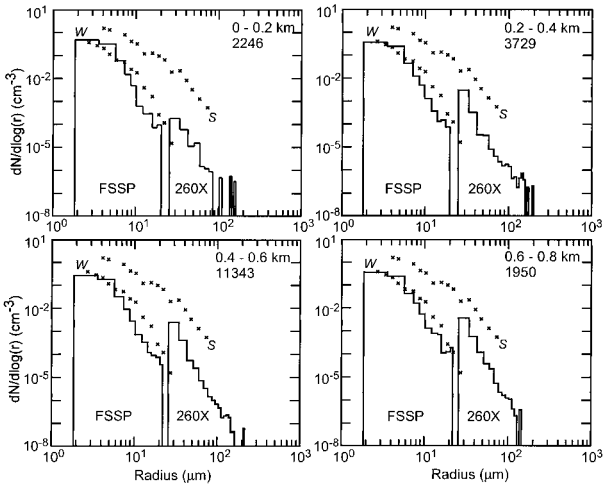

FIG. 5. SCMS clear-air composite particle size distributions derived using FSSP and 260X measurements from the surface to 0.8 km within 0.2-km layers. The number of 1-Hz samples that are included in each composite are shown. At each height, the sea-salt nuclei size data collected by Woodcock (1953) for weak (W: 0.3–1.5 m s^{-1}) and strong (S: 13.9–17.1 m s^{-1}) wind cases in the vicinity of Hawaii are overlaid for reference.

The SCMS clear-air composite particle distribution in the region near cloud base, 0.6–0.8 km, shows concentrations of particles with radii greater than 50 and 100 μm to be 0.225 and 0.002 L^{-1}, respectively. These measurements are consistent with raindrop concentrations observed during moderate rain to drizzle events and correspond to approximate rainfall rates of 1.35 and 0.012 cm h^{-1} for concentrations of 0.225 and 0.002 L^{-1} of 1-mm diameter raindrops. These measurements are consistent with results shown by Exton et al. (1983), who measured particles with radii of 80 μm at concentrations of about 0.02 L^{-1} and found a major contribution to volumetric loading for particles of radii between 10 and 80 μm.

A slight increase in the concentration of particles with radius greater than about 30 μm is apparent between the 0–0.2- and 0.2–0.4-km layers. At levels above 0.2 km, particle concentrations remain about the same to a height of 0.8 km. This result is somewhat surprising and differs from those found by previous studies (e.g., Woodcock 1953), where the concentration of large particles was found to decrease with altitude. Our reported particle sizes are sizes at the ambient relative humidity while Woodcock's were at 99% RH. This may partially account for the differences in the observations. It is also possible that residual aerosol layers from the previous day's developed boundary layer partially account for this observation. Standard statistical tests were performed to compare particle concentrations within individual size bins for the spectra at different heights. Results show that from the surface to 0.8 km the composite clear-air SCMS particle concentrations within

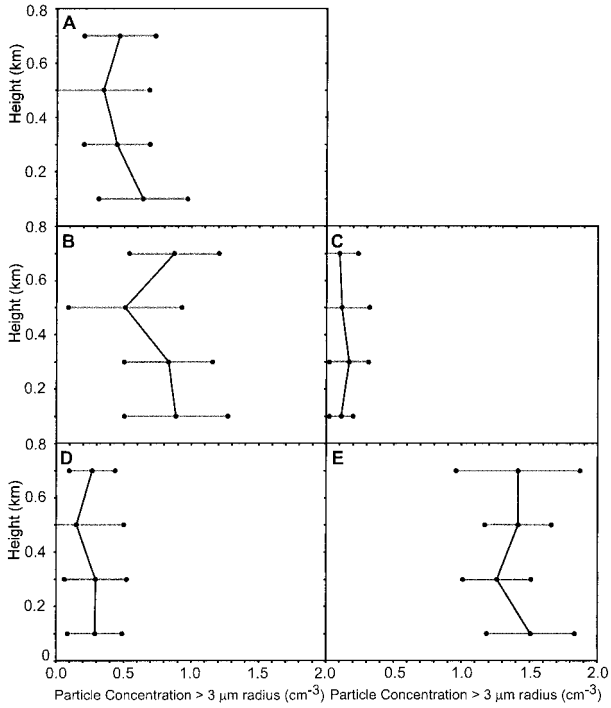

FIG. 6. Vertical profile of the mean and standard deviation of the composite total particle concentrations of particles >3-μm radius for (a) SCMS composite, (b) SCMS onshore flow days, (c) SCMS offshore flow days, (d) weak-wind onshore flow case (7 Aug 1995), and (e) strong-wind onshore flow case (31 Jul 1995).

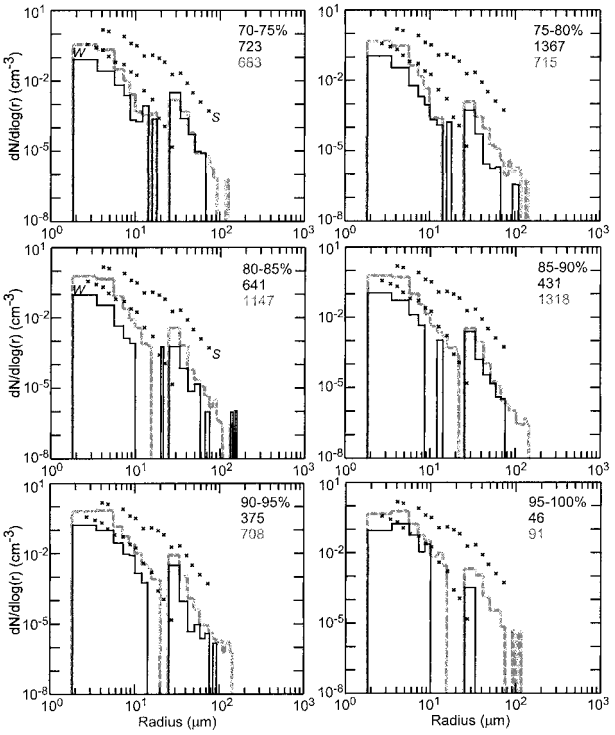

FIG. 7. Composite particle size distributions as a function of relative humidity for offshore (black) and onshore (gray) days. The number of 1-Hz samples that are included in each composite are shown. The sea-salt nuclei size data collected by Woodcock (1953) for weak (W: 0.3–1.5 m s^{-1}) and strong (S: 13.9–17.1 m s^{-1}) wind cases are overlaid for reference.

corresponding size intervals were not significantly different at a 95% confidence level. These analyses suggest that the composite particle size distributions at each level are not unique. Unlike the relative humidity analyses, there was no consistent change in the clear-air spectra with increasing height.

Figure 6a shows the SCMS clear-air mean and standard deviation of the total particle concentration of particles >3 μm for each layer determined from the 1-Hz FSSP and 260X measurements. The mean decreases with height in the three lowest layers from 0.64 to 0.35 cm^{-3} and then slightly increases in the 0.6–0.8-km layer to 0.46 cm^{-3}. However, the standard deviation at any level is about as large as the variation in the means. The decrease of the mean total concentration with height is in agreement with results of Blanchard et al. (1984) and suggests that the source of the particles is likely to be at or near the surface.

c. Wind direction variations

The SCMS data used to derive the particle size spectra in Fig. 4 were separated into two categories representing cases when winds were onshore and offshore. The offshore flow cases are more likely to be influenced by aerosol sources from the Florida peninsula. These aerosols are likely to be smaller than the smallest size detectable by the FSSP. The onshore flow cases are more likely to be dominated by aerosols of marine origin. More giant and ultragiant sea-salt aerosol should be expected for the onshore flow cases. The SCMS onshore and offshore distributions included aircraft data from 4 and 6 C130 flights, respectively. An average low-level wind direction and speed were determined from surface observations during each C130 flight period. The average wind for onshore cases was 5.5 m s^{-1} from 114° and for offshore cases was 4.0 m s^{-1} from 243°. The two remaining flights of the 12 had nearly along shore wind directions and were not used in these analyses.

Figure 7 shows a comparison of composite particle distributions for SCMS onshore versus offshore flow cases as a function of relative humidity. In general, the onshore particle distributions (gray) appear to show increased concentrations over offshore distributions (black) for relative humidities from 70% to 100%. However, except for the smallest two useable size bins of the FSSP, the differences between the onshore and offshore particle distributions were not statistically significant at the 95% confidence interval. Similar results were found when composite particle distributions for SCMS onshore versus offshore flow cases were examined as a function of height.

Figures 6b,c show that the composite values of total concentration of particles >3 μm for onshore flow cases

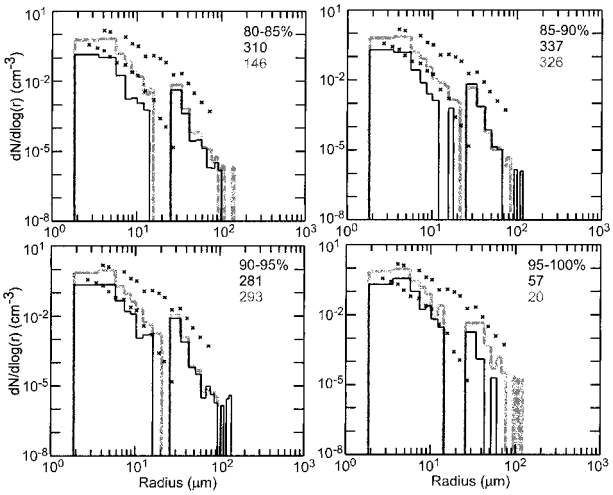

FIG. 8. Composite particle size distributions as a function of relative humidity for weak wind (black) and stronger wind (gray) days. The number of 1-Hz samples that are included in each composite are shown. The sea-salt nuclei size data collected by Woodcock (1953) for weak (W: 0.3–1.5 m s^{-1}) and strong (S: 13.9–17.1 m s^{-1}) wind cases are overlaid for reference.

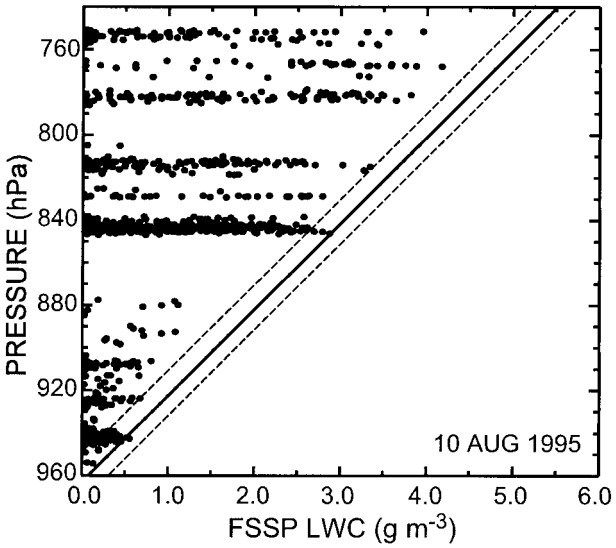

FIG. 9. Values of liquid water content derived from measurements of the FSSP for the entire C130 flight on 10 Aug 1995. The solid line represents the calculated adiabatic liquid water values. The dashed lines show the uncertainty in the calculated adiabatic values due to the uncertainty in the estimation of cloud-base temperature and pressure.

were as much as 8 times greater than those for offshore flow cases from the surface to 0.8 km. The total concentration for offshore flow cases shows only small variations with height from an average of 0.12 cm^{-3}. For the composite onshore flow, the total concentrations decreased from 0.89 cm^{-3} at the surface to 0.51 cm^{-3} in the 0.4–0.6-km layer and then increased to 0.87 cm^{-3} in the 0.6–0.8-km layer. On three of four onshore flow cases, soundings obtained by the NCAR integrated sounding system during the C130 flight period showed an inversion layer below 1.0 km. The increased concentration of particles in the 0.6–0.8-km layer may be a result of trapping of particles in the stable layer after they were transported vertically by boundary layer circulations.

d. Wind speed variations

Over oceanic and coastal regions, sea-salt aerosols are introduced through the agitation of the sea surface by the wind (De Leeuw 1986). Near Hawaii, Woodcock (1953) showed that for greater wind force a rather consistent pattern of increase in concentration and sizes of particles near cloud base was observed. Figure 8 shows a comparison of particle distributions from two SCMS onshore wind days, 7 August (weak winds at 2.6 m s^{-1} from 40°) and 31 July (stronger winds at 7.7 m s^{-1} from 70°). The results are only shown for RH >80% because insufficient samples were available at lower RH. The results show that particle concentrations in the radius range of 2–24 μm increase with wind speed. Again, the difference between the spectra were only statistically significant at the 95% confidence level for the smaller size bins of the FSSP. Similar results were also found when composite particle distributions on 7 August and 31 July were examined as a function of height. The vertical profile of total particle concentration in Figs. 6d,e show an increase by about a factor of 6 from the weak-wind to strong-wind concentrations at all levels up to 0.8 km.

4. Near-adiabatic cumulus cores

A fundamental problem that has hampered studies of the warm-rain process has been the difficulty in obtaining accurate measurements of the LWC as a function of time and space in evolving cumulus clouds. The distribution and magnitude of cloud liquid water regulates the rate at which raindrops grow. Lawson and Blyth (1998) have shown that regions of adiabatic LWC existed within small cumulus clouds observed during SCMS. This portion of our investigation examines the microphysical characteristics of near-adiabatic liquid water cores found in small cumulus clouds.

Figure 9 shows values of LWC derived from measurements of the FSSP for the entire C130 flight on 10 August 1995. The solid line on Fig. 9 represents the calculated adiabatic liquid water values. The dashed lines represent the uncertainty in the adiabatic values due to the uncertainty in the estimation of cloud base temperature and pressure. The comparison of FSSP LWC with the adiabatic values suggests the C130 penetrated several near-adiabatic cumulus cores on 10 August. For all SCMS C130 flights, the FSSP LWC data were compared with the adiabatic LWC value at flight altitude to determine the time periods of near-adiabatic

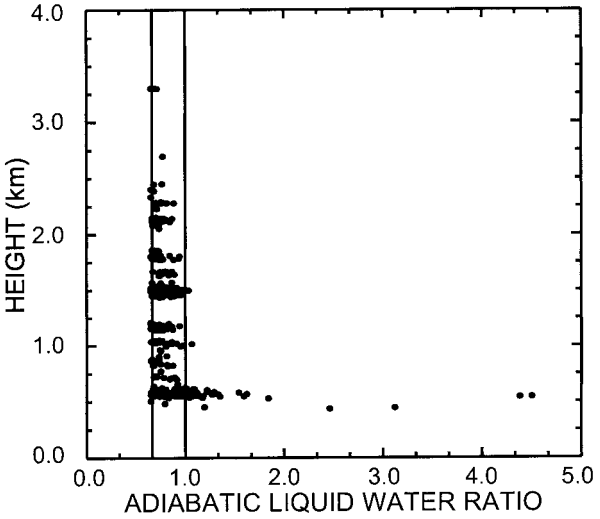

FIG. 10. Ratio of FSSP LWC to adiabatic liquid water content for all SCMS near-adiabatic cumulus core penetrations.

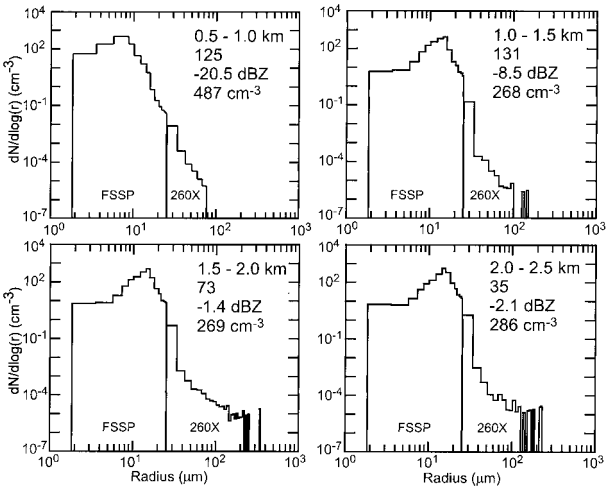

FIG. 11. SCMS composite drop distributions as a function of height. The height interval, number of 1-Hz samples, calculated reflectivity, and total cloud droplet concentration are included for each distribution.

penetrations. Near-adiabatic penetrations were arbitrarily defined as having a FSSP LWC of greater than 66% of the adiabatic value and vertical motions greater than or equal to zero. Using this threshold, 175 SCMS cloud penetrations during 10 C130 flights had near-adiabatic cores. The average duration within a core was approximately 2.1 s, suggesting that the average diameter of a small cumulus near-adiabatic core observed during SCMS was at least 220 m.

Figure 10 shows the vertical distribution of the ratio of FSSP LWC to adiabatic liquid water for the 373 data points where the FSSP LWC met or exceeded the near-adiabatic threshold. Approximately 51% of the LWC measurements above the threshold were greater than 75% of the adiabatic value and about 18% exceeded 90% of the adiabatic value. About 9% of the ratios were larger than unity (superadiabatic). These were almost all located near cloud base where errors in the ratio are maximized due to the uncertainty in cloud-base temperature and pressure.

Composite droplet distributions were constructed using data within the near-adiabatic cores to examine the microphysical properties of near-adiabatic cores in small cumulus clouds. Figure 11 shows the SCMS composite droplet distributions as a function of height in 0.5-km intervals, from near cloud base (0.5–1.0-km height) to 2.5 km. The 2.5-km level was typically the highest level at which near-adiabatic LWC cores were observed by the C130. This level was about two-thirds of the distance to the final height typically achieved by these clouds. The results suggest a physically consistent evolution of the droplet distribution with height in the near-adiabatic cores. The diameter of the peak in the small drop distribution increases from the near cloud-base level to the 1.0–1.5 level and then remains relatively unchanged with height. This behavior is expected from diffusional growth where 1) water vapor condenses on the smaller aerosol causing rapid growth rates of the droplets near cloud base, and 2) the growth rate for these droplets slows as their radius increases. For precipitation to develop within observed timescales of 15–20 min, it is very important that larger drops be present for the collision-coalescence process to proceed. Larger droplets between 20- and 75-μm radius were observed just above cloud base in the near-adiabatic cores. Again, the distribution of these drops was exponential. There were no drops >100 μm just above cloud base, implying that artifacts associated with shedding were not contaminating the data. Larger drops appeared at higher altitudes. The increased concentration of the larger drops must be due to the accretion process, since diffusional growth is much too slow to account for the change. Based on this data, accretional growth must clearly begin very close to cloud base. The analyses suggest that the larger drops are due to the presence of giant and ultragiant aerosols observed in the clear air. However, modeling results will provide a better test of the hypothesis that the large drops result from the growth on giant and ultragiant aerosols.

Figure 12 shows the vertical distribution of vertical velocity within the near-adiabatic cores. The scatter of the measurements is large. There are even a few measurements where the vertical motions are near zero. It is possible that these measurements were near the edge of the near-adiabatic cores, or that several of the sampled cores had completed their ascent but had not yet undergone significant entrainment. Unfortunately, from the measurements, we were unable to clearly evaluate the stage of growth of the cumuli containing these near-adiabatic cores at the time of individual aircraft penetrations. Nearly 50% of the observations within cumulus cores were collected at two flight levels, near cloud base and at approximately 1.5 km. Figure 11 includes the

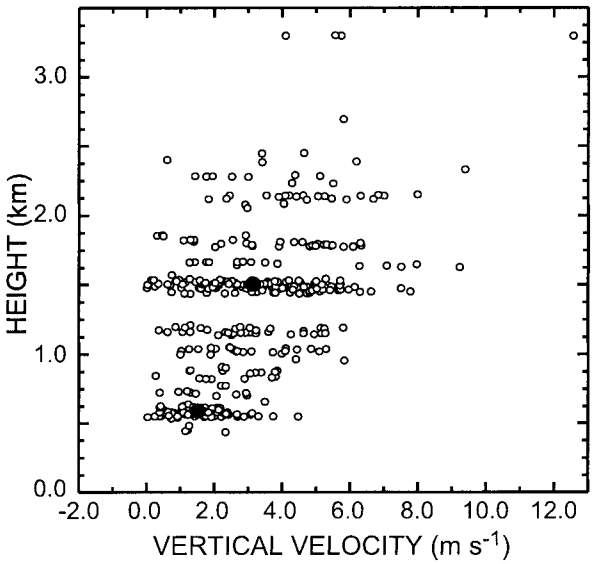

FIG. 12. Vertical distribution of vertical velocity within SCMS near-adiabatic cores from aircraft in situ measurements. The averages from the 0.5–0.7- and 1.4–1.6-km layers are shown by solid circles.

averages from the 0.5–0.7- and 1.4–1.6-km layers of 1.57 and 3.36 m s^{-1}, respectively.

5. Comparison of radar reflectivity with composite droplet distributions

In this section, we compare the reflectivity calculated from the aircraft composite droplet distributions with the X-band radar reflectivity of two clouds. The first on 5 August reached a lower altitude, developed a maximum radar reflectivity of approximately −6 dB*Z* (cloud 1, Figs. 13a–d), and was found to contain a near-adiabatic core by the C130. The second, cloud 2, on 10 August grew to a higher altitude and reached a maximum radar reflectivity of about 24 dB*Z*. The purpose of this comparison is to further evaluate the representativeness of the large-size end of composite droplet distributions. Since the Rayleigh radar reflectivity (represented here by X-band reflectivity) is proportional to the summation of ND^6 (see Knight and Miller 1998), it is primarily determined by the middle- and large-sized droplets.

The composite drop distributions from near-adiabatic cores (Fig. 11) encompass a range of conditions associated with the early stage of cumulus growth. There was unavoidable natural variability associated with the cloud-base height, cloud depth, and other factors. In general, aircraft penetrations of a cloud only occurred after the cloud had grown sufficiently so that the aircraft scientist could visually identify it as a reasonable target cloud. Additional time was then required for the aircraft to arrive at the cloud. For this reason, most of the cloud penetrations occurred several minutes into the growth of the cloud. In clouds similar to the examples shown in Fig. 13, penetrations typically occurred at stages shown in Figs. 13b,c,f,g. We therefore compare the reflectivity calculated from the composite droplet distributions with the radar reflectivity observed at these stages of cloud growth.

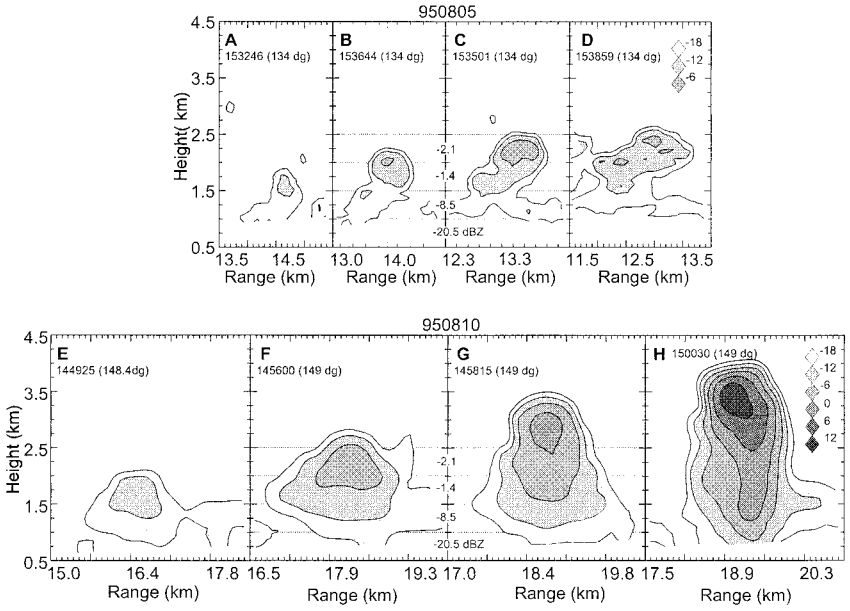

FIG. 13. NCAR CP2 X-band radar reflectivity evolution of two small cumulus clouds on 5 and 10 Aug 1995. Reflectivity calculated from SCMS composite droplet distributions are shown for their corresponding 0.5-km layers (see Fig. 8) on (B), (C), (F), and (G). Radar scan times (UTC) and azimuth angle are shown for each panel.

The cloud-base height of cloud 1 was estimated to be about 1.0 km. The radar reflectivity near cloud base (−18 dB*Z*) agreed well with the reflectivity from the composite spectra in the cloud-base layer (−20.5 dB*Z*). For heights between 1.0 and 2.5 km, the radar reflectivity was lower by about 3–8 dB*Z*. Cloud base of cloud 2 was estimated to be about 0.8 km. In this case there was very good agreement between the reflectivity from cloud base to 2.5 km (Figs. 13f,g) with the reflectivity from the composite droplet distributions.

The two clouds selected demonstrate the variability in cloud structure and evolution that was encountered by the aircraft during sampling. There is obviously a great deal of uncertainty involved in the comparison of composite aircraft droplet distributions from an entire project with the observed radar reflectivity of individual clouds. Nevertheless, the comparisons provide independent evidence that the composite droplet distributions reasonably represent the evolving microstructure of the cores of small cumulus clouds as they grow vertically. The composite droplet distributions, the observed rapid evolution of the radar reflectivity as the clouds grow (e.g., Fig. 13), and the comparisons between them provide strong evidence of a rapid precipitation growth process that appears to be triggered by the ultragiant nuclei entering cloud base.

6. Summary and conclusions

The purpose of this investigation was to examine the microphysical processes that lead to the development of precipitation in small, warm, Florida cumulus. The data used for this investigation were from the Small Cumulus Microphysics Study (SCMS), which was conducted along the east central Florida coast in the summer of 1995.

Aircraft measurements from the NCAR C130 were used to determine the concentration and size distribution of giant and ultragiant nuclei in clear air as a function of relative humidity, altitude, wind speed, and wind direction. Data from 12 flights were composited to greatly improve the sampling statistics for the clear-air particle size distributions, particularly for the larger particles that have low concentrations. The clear-air particle distributions show that ultragiant particles exist from the surface to cloud base in concentrations that correspond to the concentrations of raindrops observed during drizzle to moderate rainfall events. A shift of the spectra toward larger size with increasing relative humidity was observed, suggesting that the spectra are composed of deliquesced particles growing by condensation. These particles had radii extending from 10 to 150 μm and, based on comparisons with independent measurements in marine environments, are likely to have been composed largely of sea-salt nuclei. The independent measurements of particle size distributions in marine environments (Fig. 1) compare well with SCMS particle distributions.

The data presented in this article demonstrate that many small Florida cumulus clouds contained cores where the observed liquid water content was greater than 66% of the adiabatic value. The evolution of the cloud droplet distribution within the near-adiabatic cores as a function of height showed the expected increase in the small droplet mode associated with condensation and an increase in the concentration of larger droplets expected from growth by accretion. Measurements of droplet distributions in the near-adiabatic cores of SCMS cumulus clouds show droplets with radii extending above 70 μm even near cloud base. These measurements are consistent with the clear-air measurements and provide further evidence that the ultragiant nuclei can immediately act as embryos for raindrop growth by accretion upon entering cloud base. Comparisons with radar reflectivity data provided independent evidence that the composite droplet distributions reasonably represent the evolving microstructure of the cores of small cumulus clouds as they grow vertically.

The analyses presented in this article provide strong evidence of an efficient process for the initial development of precipitation in warm Florida cumuli. Taken together, these data support a conceptual model of the raindrop formation process that is simple and efficient and corresponds to the early ideas proposed by Woodcock (1952) and explored further by Woodcock (1953), Ochs and Semonin (1979), Johnson (1982, 1993), and Szumowski et al. (1999). This model consists of raindrop embryo formation on sea-salt nuclei followed by immediate growth by accretion as newly formed drops proceed upward through near-adiabatic cores of cumulus clouds.

Acknowledgments. The authors appreciate the very helpful comments and suggestions of David Johnson and an anonymous reviewer for greatly improving the manuscript. We would like to thank all the scientists, staff, engineers, and technicians that participated in the Small Cumulus Microphysics Study to make it a successful field project. We appreciate the efforts of Charlie Knight in coordinating the SCMS and making the C130 videos available. We also thank Chris Webster and Ron Ruth for their efforts in reprocessing the original NCAR C130 dataset for SCMS. Computing support was provided by NCAR Scientific Computing Division. Funding support for participation in SCMS and this research was provided by the National Science Foundation under research Grants ATM 9223165 and ATM 9634660.

REFERENCES

Austin, P. H., S. Siems, and Y. Wang, 1995: Constraints on droplet growth in radiatively cooled stratocumulus clouds. *J. Geophys. Res.,* **100,** 14 231–14 242.

Baker, M. B., and J. Latham, 1979: The evolution of droplet spectra and rate of production of embryonic raindrops in small cumulus clouds. *J. Atmos. Sci.,* **36,** 1612–1615.

Baumgardner, D., 1989: Airborne measurements for cloud micro-

physics. NCAR RAF Bull. 24, 22 pp. [Available from NCAR Research Aviation Facility, P.O. Box 3000, Boulder, CO 80307.]
Beard, K. V., and H. T. Ochs III, 1993: Warm-rain initiation: An overview of microphysical mechanisms. *J. Appl. Meteor.,* **32,** 608–625.
Blanchard, D. C., A. H. Woodcock, and R. J. Cipriano, 1984: The vertical distribution of the concentration of sea salt in the marine atmosphere near Hawaii. *Tellus,* **36B,** 118–125.
Charlson, R. J., J. E. Lovelock, M. O. Andreae, and S. G. Warren, 1987: Oceanic plankton, atmospheric sulfur, cloud albedo and climate. *Nature,* **326,** 655–661.
Cooper, W. A., D. Baumgardner, and J. E. Dye, 1986: Evolution of the droplet spectra in Hawaiian orographic clouds. Preprints, *Conf. on Cloud Physics,* Snowmass, CO, Amer. Meteor. Soc., 52–55.
Cornford, S. G., 1967: Sampling errors in measurements of raindrop and cloud droplet concentrations. *Meteor. Mag.,* **96,** 271–282.
de Leeuw, G., 1986: Vertical profiles of giant particles close above the sea surface. *Tellus,* **38B,** 51–61.
Exton, H. J., J. Latham, P. M. Park, M. H. Smith, and R. R. Allan, 1983: The production and dispersal of maritime aerosol. *Oceanic Whitecaps and Their Role in Air–Sea Exchange Processes,* E. C. Monahan and G. Mac Niocaill, Eds., D. Reidel, 175–193.
Feingold, G., W. R. Cotton, S. M. Kreidenweis, and J. T. Davis, 1999: The impact of giant cloud condensation nuclei on drizzle formation in stratocumulus: Implications for cloud radiative properties. *J. Atmos Sci.,* **56,** 4100–4117.
Fitzgerald, J. W., 1991: Marine aerosols: A review. *Atmos. Environ.,* **25A,** 533–545.
Hegg, D. A., L. F. Radke, and P. V. Hobbs, 1991: Measurements of Aitken nuclei and cloud condensation nuclei in the marine atmosphere and their relationship to the DMS-cloud-climate hypothesis. *J. Geophys. Res.,* **96,** 18 727–18 733.
Hoppel, W. A., 1987: Nucleation in the MSA-water vapor system. *Atmos. Environ.,* **21,** 2703–2709.
——, J. W. Fitzgerald, G. M. Frick, R. E. Larson, and E. J. Mack, 1989: Atmospheric aerosol size distributions and optical properties in the marine boundary layer over the Atlantic Ocean. NRL Rep. 9188, 81 pp. [Available from Naval Research Laboratory, 4555 Overlook Ave. SW, Washington, DC 20375; also available online at http://infoweb.nrl.navy.mil/webcat.html.]
Inman, R. L., 1969: Computation of temperature at the lifted condensation level. *J. Appl. Meteor.,* **8,** 155–158.
Johnson, D. B., 1979: The role of coalescence nuclei in warm rain initiation. University of Chicago Dept. of Geophysical Sciences Tech. Note 55, 119 pp. [Available from Dept. of Geophysical Sciences, University of Chicago, 5734 S. Ellis Ave., Chicago, IL 60637.]
——, 1982: The role of giant and ultragiant aerosol particles in warm rain initiation. *J. Atmos. Sci.,* **39,** 448–460.
——, 1993: The onset of effective coalescence growth in convective clouds. *Quart. J. Roy. Meteor. Soc.,* **119,** 925–933.
Khain, A. P., and M. B. Pinsky, 1995: Drop inertia and its contribution to turbulent coalescence in convective clouds. Part I: Drop fall in the flow with random horizontal velocity. *J. Atmos. Sci.,* **52,** 196–206.
Knight, C. A., and L. J. Miller, 1993: First radar echoes from cumulus clouds. *Bull. Amer. Meteor. Soc.,* **74,** 179–188.
——, and ——, 1998: Early radar echoes from small, warm cumulus: Bragg and hydrometeor scattering. *J. Atmos. Sci.,* **55,** 2974–2992.
Knollenberg, R. G., 1981: Techniques for probing cloud microstructure. *Clouds, Their Formation, Optical Properties and Effects,* P. V. Hobbs and A. Deepak, Eds., Academic Press, 15–92.
Kogan, Y. L., 1993: Drop size separation in numerically simulated convective clouds and its effect on warm rain formation. *J. Atmos. Sci.,* **50,** 1238–1253.
Korolev, A. V., 1995: The influence of supersaturation fluctuations on droplet size spectra formation. *J. Atmos. Sci.,* **52,** 3620–3634.
Latham, J., and R. L. Reed, 1977: Laboratory studies of the effects of mixing on the evolution of cloud droplet spectra. *Quart. J. Roy. Meteor. Soc.,* **103,** 297–306.
Lawson, R. P., and A. M. Blyth, 1998: A comparison of optical measurements of liquid water content and drop size distribution in adiabatic regions of Florida cumuli. *Atmos. Res.,* **47,** 671–690.
Ludlam, F. H., and P. M. Saunders, 1956: Shower formation in large cumulus. *Tellus,* **8,** 424–442.
Meszaros, A., and K. Vissy, 1974: Concentration, size distribution and chemical nature of atmospheric aerosol particles in remote ocean areas. *J. Aerosol Sci.,* **5,** 101–109.
Mordy, W., 1959: Computations of the growth by condensation of a population of cloud droplets. *Tellus,* **11,** 16–44.
Ochs, H. T., III, and C. S. Yao, 1978: Moment-conserving techniques for warm cloud microphysical computations. Part I: Numerical techniques. *J. Atmos. Sci.,* **35,** 1947–1958.
——, and R. G. Semonin, 1979: Sensitivity of a cloud microphysical model to an urban environment. *J. Appl. Meteor.,* **18,** 1118–1129.
O'Dowd, C. D., M. H. Smith, I. E. Consterdine, and J. A. Lowe, 1997: Marine aerosol, sea-salt, and the marine sulphur cycle: A short review. *Atmos. Environ.,* **31,** 73–80.
Politovich, M. K., and W. A. Cooper, 1988: Variability of the supersaturation in cumulus clouds. *J. Atmos. Sci.,* **45,** 1651–1664.
Pruppacher, H. R., and J. D. Klett, 1978: *Microphysics of Clouds and Precipitation.* D. Reidel, 714 pp.
Rauber, R. M., K. V. Beard, and B. M. Andrews, 1991: A mechanism for giant raindrop formation in warm, shallow convective clouds. *J. Atmos. Sci.,* **48,** 1791–1797.
Rogers, R. R., and M. K. Yau, 1989: *A Short Course in Cloud Physics.* Pergamon Press, 293 pp.
Szumowski, M. J., R. M. Rauber, and H. T. Ochs III, 1999: The microphysical structure and evolution of Hawaiian rainband clouds. Part III: A test of the ultragiant nuclei hypothesis. *J. Atmos. Sci.,* **56,** 1980–2003.
Telford, J. W., T. S. Keck, and S. K. Chai, 1984: Entrainment at cloud tops and the droplet spectra. *J. Atmos. Sci.,* **41,** 3170–3179.
Warner, J., 1955: The water content of cumuliform cloud. *Tellus,* **7,** 449–457.
Woodcock, A. H., 1952: Atmospheric salt particles and raindrops. *J. Meteor.,* **9,** 200–212.
——, 1953: Salt nuclei in marine air as a function of altitude and wind force. *J. Meteor.,* **10,** 362–371.
——, and M. M. Gifford, 1949: Sampling atmospheric sea-salt nuclei over the ocean. *J. Mar. Res.,* **8,** 177–197.
——, R. A. Duce, and J. L. Moyers, 1971: Salt particles and raindrops in Hawaii. *J. Atmos. Sci.,* **28,** 1252–1257.